

PACS 61.46.–w, 64.70.Nd, 82.80.Rt

## Oxygen ion-beam modification of vanadium oxide films for reaching a high value of the resistance temperature coefficient

T.M. Sabov, O.S. Oberemok, O.V. Dubikovskiy, V.P. Melnik, V.P. Kladko, B.M. Romanyuk, V.G. Popov, O.Yo. Gudymenko, N.V. Safriuk

*V. Lashkaryov Institute of Semiconductor Physics, NAS of Ukraine,  
41, prospect Nauky, 03028 Kyiv, Ukraine;  
e-mail: romb@isp.kiev.ua*

**Abstract.** A new method to prepare vanadium oxide with a high temperature coefficient of resistance (TCR) and low resistance for uncooled micro-bolometers has been proposed. Amorphous vanadium oxide films with  $V_2O_3$  phase inclusions have been fabricated on silicon and silica substrates at the temperature 200 °C by using the direct current reactive magnetron sputtering method in controlled Ar/O<sub>2</sub> atmosphere. Additional oxygen ion implantation in the deposited films allows to synthesize vanadium oxide with crystalline inclusions of VO<sub>2</sub> and V<sub>2</sub>O<sub>5</sub> phases under the low temperature annealing. The following long low-temperature annealing provides formation of VO<sub>x</sub> (at  $x \rightarrow 2$ ) film with the TCR close to 7.0%/°C.

**Keywords:** resistance temperature coefficient, vanadium oxide films, reactive magnetron sputtering, low-temperature annealing, oxygen implantation.

Manuscript received 25.01.17; revised version received 20.04.17; accepted for publication 14.06.17; published online 18.07.17.

### 1. Introduction

The vanadium oxide films are promising material for uncooled micro-bolometers with a low noise level. These devices are commercially attractive for military use as night vision, medical imaging, *etc.*, [1]. Infrared (IR) sensitivity of the VO<sub>x</sub> films (at  $x \rightarrow 2$ ) is related with the enormous changes in the electrical resistance and optical absorption spectra caused by semiconductor-to-metal phase transition (SMT). Since the vanadium oxide exists in multiple phases, SMT temperatures are different for each phase: V<sub>2</sub>O<sub>3</sub> (~–113 °C), VO<sub>2</sub> (~68 °C), V<sub>2</sub>O<sub>5</sub> (within the range 256 to 286 °C) [2-4]. For uncooled micro-bolometers it is important to obtain a high TCR value near the room temperature. Only vanadium dioxide has SMT in this temperature range. So, availability of a sufficient amount of VO<sub>2</sub> crystallites

in the VO<sub>x</sub> film is necessary for high IR sensitivity of this type devices. Most of commercial micro-bolometers are constructed on the base of polycrystalline VO<sub>x</sub> films that contain a mixture of VO, V<sub>2</sub>O<sub>3</sub>, VO<sub>2</sub>, V<sub>2</sub>O<sub>5</sub> and other phases. It leads to the electric shunting or isolation of VO<sub>2</sub> crystallites. That restricts the TCR value and, consequently, the device sensitivity, and leads to increased noise [5].

The vanadium dioxide SMT is related with the crystal structure geometric transformation from the monoclinic to tetragonal syngony. These atomic displacements lead to changes in the electronic structure causing the valence and conduction band “overlapping” [6]. SMT is accompanied by the occurrence of significant elastic stresses. It leads to the destruction of bulk crystals [7]. Therefore, most of practical vanadium dioxide applications are related with thin nanostructured

films (100...200 nm). They are not destroyed during the thermal cycling and allow reducing the SMT temperature. Thus, the TCR value depends on the quantity, size and type of crystallites in the film. Obviously, the grain interfaces also effect on the TCR value. Numerous methods were used for preparation of VO<sub>x</sub> films with majority of VO<sub>2</sub> nanocrystallites for a high TCR value. In most of the cases, grown and annealed VO<sub>x</sub> films exhibit TCR values within the range 2...3%/K [3, 8]. Additional doping the VO<sub>x</sub> films with tungsten enables to increase the TCR up to 4%/K [9]. Also, it was shown that the VO<sub>x</sub> film resistance is reduced without changing of the TCR values after hydrogen ion implantation with subsequent annealing at 300 °C [10]. DC magnetron sputtering is the most commercially attractive method for preparing the VO<sub>x</sub> film. In our previous work [11], the method of low temperature deposition (250...300 °C) with the following low temperature annealing (300 °C) was proposed for high-ordered VO<sub>2</sub> phase formation [12] and VO<sub>x</sub> film synthesis with the high TCR value (~7%/K) [13].

To successfully implement this method, before the annealing stage it is important to have an amorphous VO<sub>x</sub> (1.8 < x < 2.2) film with rare inclusions of VO<sub>2</sub> and V<sub>2</sub>O<sub>3</sub> crystallites. For obtaining the required functional properties of the film, it can be used the low-temperature annealing mode (depending on the x value), which provides controlled growth of certain vanadium oxide phases. Preparation of the VO<sub>x</sub> film with a certain x value is a complex task, because this parameter is very sensitive to the slightest changes in the deposition conditions.

In this paper, we propose to adjust the component composition of the deposited film by oxygen ion implantation to form the film with a high TCR value during annealing.

## 2. Experimental

Vanadium oxide films were deposited on the heated (200 °C) silicon and silica substrates by using the DC magnetron sputtering system. The gas discharge of oxygen-argon mixture was used for sputtering the 99.95% purity vanadium target. The reactor chamber was pumped out to the pressure 3·10<sup>-6</sup> Torr before film deposition. The distance between the target and substrate was approximately 50 mm. The operation gas pressure was maintained at 4·10<sup>-3</sup> Torr with addition of 1% oxygen. The resulting films had a dominant V<sub>2</sub>O<sub>3</sub> structure with the thickness close to 300 nm. The additional oxygen is required for V<sub>2</sub>O<sub>3</sub> to VO<sub>2</sub> structure transformation of deposited films. For this purpose, additional doping was carried out using ion implantation. The deposited films were implanted with O<sub>2</sub><sup>+</sup> ions during the subsequent annealing at 320 °C for 30+180 min. The ion implantation energy and doses were determined from the SRIM software computation. In our case, 100 keV energy and the three doses of 1·10<sup>17</sup> (low), 2·10<sup>17</sup>

(medium) and 3·10<sup>17</sup> (high) cm<sup>-2</sup> were used. The temperature dependences of the film specific electrical resistance were measured to determine the TCR values. The film thickness was measured by Dektak 3030 stylus profiler. The film crystalline structure was examined by scanning electron microscopy (SEM) and X-ray diffraction. Glancing incidence angle (1°) X-ray diffraction (GIXRD) was carried out using X'Pert PRO MPD diffractometer with the CuKα wavelength (λ = 0.15418 nm). The grain size and surface morphology of vanadium oxide films were investigated using SEM. The film structure by the depth was studied using cross-section SEM images after cutting the focused ion beam. Depth distributions for different components (Si, V, VO, V<sub>2</sub>O<sub>3</sub>, VO<sub>2</sub> and V<sub>2</sub>O<sub>5</sub>) in the films were measured by time-of-flight secondary ion mass spectroscopy (TOF-SIMS 5) by using 0.6 keV Cs sputtering.

## 3. Results and discussion

SRIM calculation of depth profiles for the oxygen-implanted VO<sub>x</sub> film (at x = 0.2 and density 4 g/cm<sup>3</sup>) are shown in Fig. 1. It is seen that the dose increase leads to compaction of the buried layer. The oxygen concentration is increased near the distribution maximum. The layer extends from 100 nm (low dose) to 130 nm (medium dose) and to 150 nm (high dose) at 1·10<sup>22</sup> cm<sup>-3</sup> oxygen concentration level. The oxygen concentrations in the formed VO<sub>x</sub> layer were 30, 50 and 65 at.%, respectively.

The TCR values were determined from the temperature dependence of specific electrical resistance by the formula:

$$TCR = \frac{1}{R_{ref}} \frac{\Delta R}{\Delta T},$$

where *R* is the specific electrical resistance of the thin film at the temperature *T*.

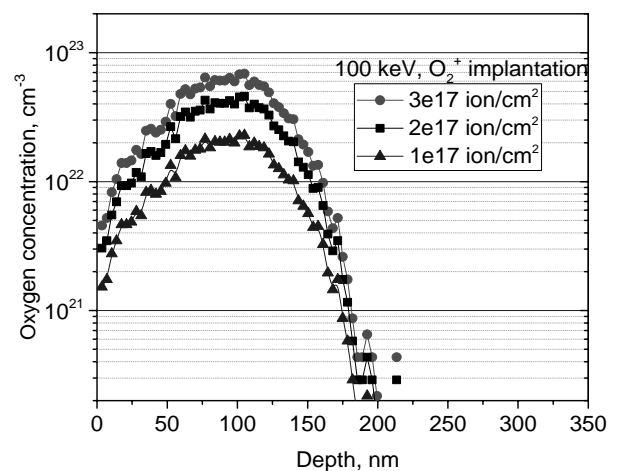


**Fig. 1.** SRIM calculation of oxygen depth profiles in V<sub>2</sub>O<sub>3</sub> film.

Low-dose oxygen implantation of  $\text{VO}_x$  films does not allow to obtain acceptable TCR values for any thermal annealing. Obviously, it is caused by a too low concentration of oxygen for generation of a sufficient amount of  $\text{VO}_2$  or  $\text{V}_2\text{O}_5$  crystallites. The temperature dependences of the film specific electrical resistance are shown for the medium (Fig. 2a) and high (Fig. 2b) oxygen doses after 30 min temperature annealing. It is seen that these dependences have a typical descending form. The electrical resistance is changed by 2 to 3 times under sample heating/cooling within the temperature range 25...60 °C. It indicates the appearance of a large number of  $\text{VO}_2$  and  $\text{V}_2\text{O}_5$  phase inclusions in the initially metallic  $\text{VO}_x$  film. The calculated TCR values within the temperature range 25...50 °C are 1.85 and 2.05 for

medium and high oxygen doses, respectively. The additional three-hour thermal annealing leads to a more abrupt change in the electrical resistance for the film implanted with the medium oxygen dose (Fig. 2c). It is seen that SMT is observed at a lower temperature.

At the same time, a film implanted with a high oxygen dose does not show any significant change in the temperature dependence of the specific electrical resistance under heating (Fig. 2d). However, the shape of investigated dependence becomes a more linear upon cooling the film.

The calculated TCR shows a strong increase of its value for the medium dose and a slight decrease for a high dose of implanted oxygen. The calculated TCR values are given in Table for several temperature ranges.

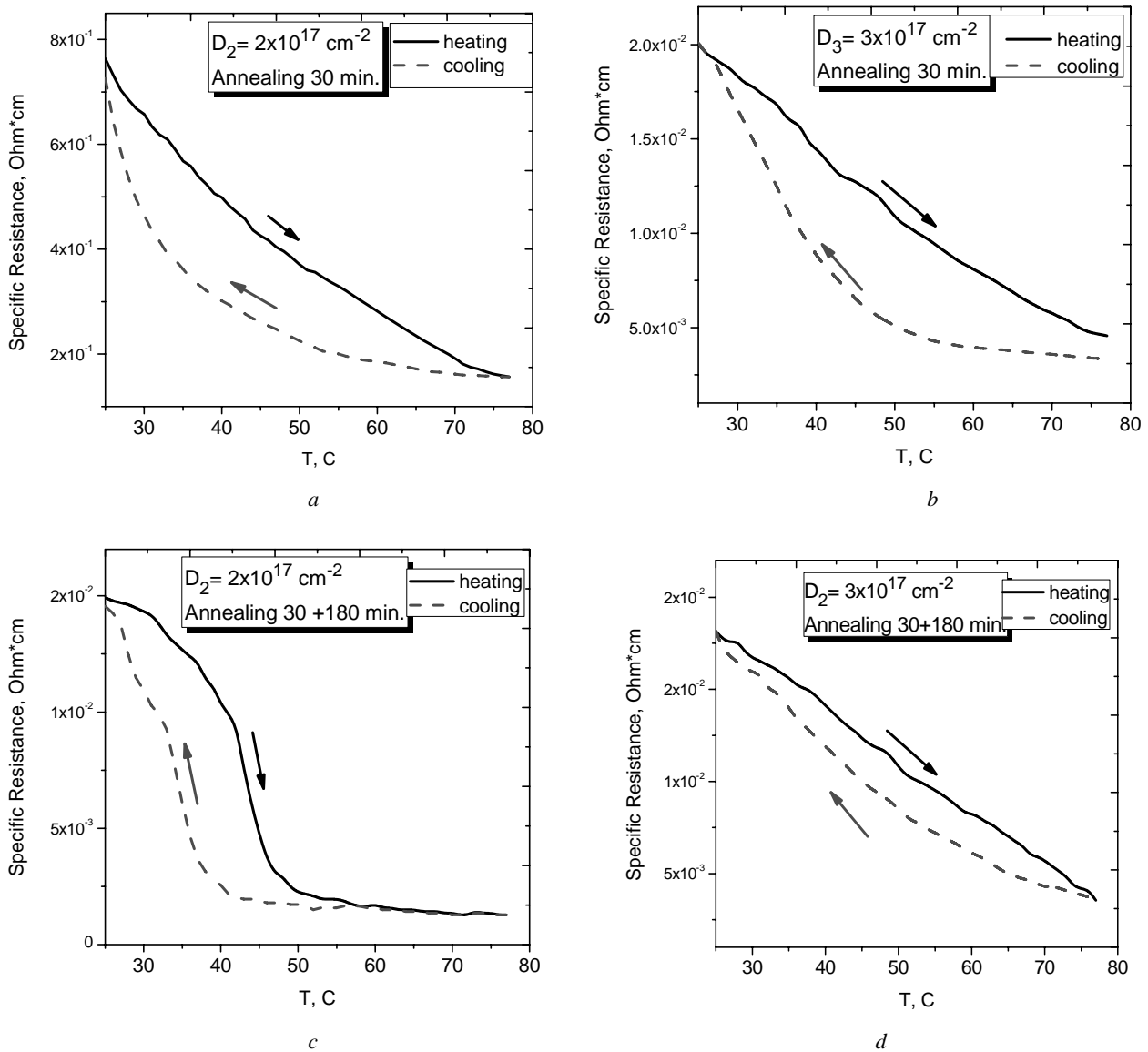


**Fig. 2.** Temperature dependence of the specific resistance for  $\text{VO}_x$  films after annealing that follows oxygen implantation with a medium (a, c) and high doses (b, d).

**Table. Calculated TCR values for some temperature ranges.**

Dose, cm <sup>-2</sup>	Annealing time, min	Temperature range, °C					
		25–35	35–45	25–45	30–40	40–50	25–50
		TCR value					
2·10 <sup>17</sup>	30	1.57	2.44	1.82	2.09	2.49	1.85
3·10 <sup>17</sup>	30	2.55	2.51	2.21	2.42	2.56	2.06
<b>2·10<sup>17</sup></b>	<b>30+180</b>	<b>1.51</b>	<b>6.27</b>	<b>3.42</b>	<b>2.77</b>	<b>7.83</b>	<b>3.40</b>
3·10 <sup>17</sup>	30+180	1.40	2.10	1.60	1.55	2.35	1.62

It is seen that the additional annealing for the medium oxygen dose implanted film leads to increase in the average TCR value up to 3.4% in the 25...50 °C temperature range. The TCR value exceeds 6% at the temperatures above 35 °C.

XRD spectra of implanted with the medium and high oxygen doses VO<sub>x</sub> films are shown in Fig. 3a and Fig. 3b, respectively. In addition, shown there are the images of fingerprint reflexes of V<sub>2</sub>O<sub>3</sub>, VO<sub>2</sub> and V<sub>2</sub>O<sub>5</sub> phases. It is seen that all the spectra have the Gauss distribution of intensity in the angle range 2θ = 20...40°. It corresponds to amorphous phase of VO<sub>x</sub> films. Also, all the spectra contain characteristic reflections of V<sub>2</sub>O<sub>3</sub> metallic phase. The main 012 reflex is observed at the angle 24.3° against the background of amorphous Gaussian distribution for the medium oxygen dose. Reflexes 024, 104, 006 and 116 are registered in the spectrum distinctly. The 30-min film annealing leads to the some peak attenuation of these reflexes in the spectrum. At the same time, we observe some reflexes indicating VO<sub>2</sub> phase formation. The reflex 200 at the angle 37° is the most clearly pronounced. Also, presented in the spectrum are reflexes 212 and 211 at the angles 42° and 55.2°, respectively. The weak 011 reflex at the angle 27.7° is observed against the background of Gaussian scattering from the amorphous phase. The appearance of peaks corresponding to weak reflexes (111 and 411) from the V<sub>2</sub>O<sub>5</sub> phase is also observed. The

main 110 reflex peak inherent to the V<sub>2</sub>O<sub>5</sub> phase is not observed, which is caused by the strong X-ray scattering from the amorphous phase. Additional annealing for 180 min leads to an increase of the reflexes intensity from the VO<sub>2</sub> phase as well as attenuation of reflexes from the V<sub>2</sub>O<sub>3</sub> and V<sub>2</sub>O<sub>5</sub> phases.

V<sub>2</sub>O<sub>3</sub> phase reflexes have lower peak intensities for the film implanted with a high dose of oxygen. The 30-min film annealing leads to some peak attenuation and extension of these reflexes in the spectrum. Obviously, it is related with the appearance of compressive and tensile stresses or with a dilution of V<sub>2</sub>O<sub>3</sub> crystallites during oxygen redistribution. Additional annealing for 180 min leads to 024 reflex appearance and narrowing the peaks of all reflexes.

This may be caused by coarsening or/and coalescence of smaller crystallites. The reflexes of VO<sub>2</sub> or V<sub>2</sub>O<sub>5</sub> phases are not found in the XRD spectrum after annealing. The average crystallite sizes with V<sub>2</sub>O<sub>3</sub> and VO<sub>2</sub> phases were estimated for both films by using the XRD spectra. The 116 reflex from V<sub>2</sub>O<sub>3</sub> phase is most clearly appeared in all the spectra, so this reflex was used for calculation of grain sizes for all the samples Fig. 4a. As we can see from Fig. 4, the grain sizes are reduced after annealing in both films. But grains are larger in the case of lower implantation dose. At the same time, the grain size of the additional VO<sub>2</sub> phase increases after annealing Fig. 4b.

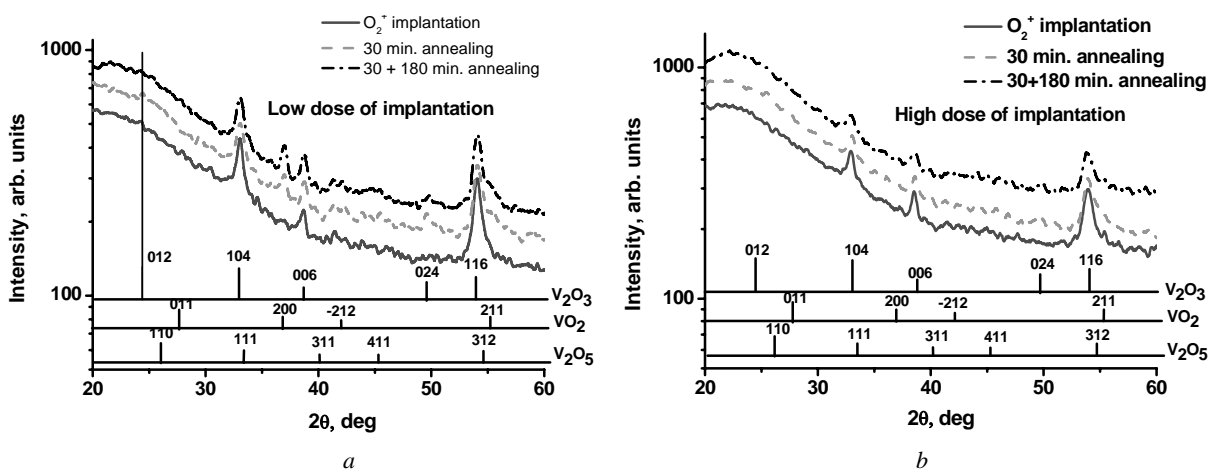


**Fig. 3.** XRD spectra of oxygen-implanted VO<sub>x</sub> films with the medium (a) and high (b) doses after implantation; 30 min annealing and 30+180 min annealing.

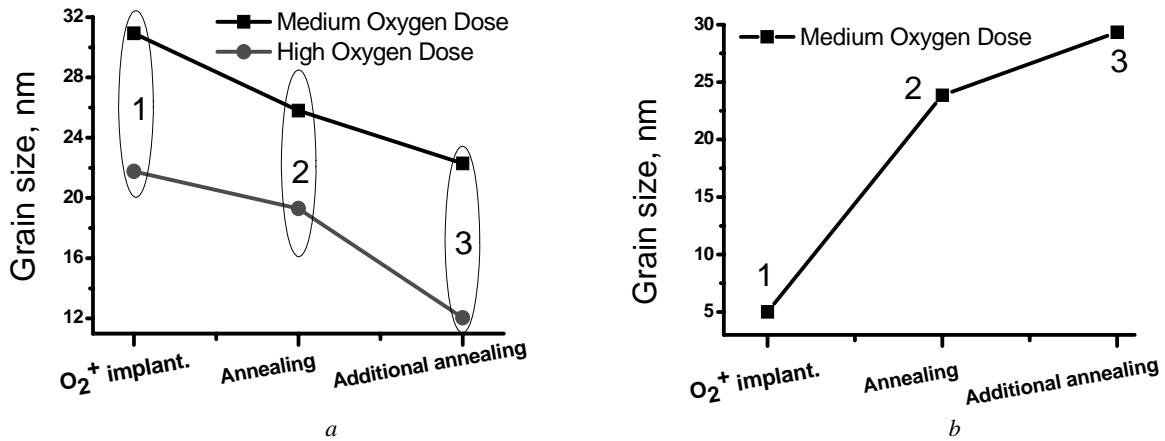


**Fig. 4.** Grain size of V<sub>2</sub>O<sub>3</sub> phase calculated from 116 reflex (a) and of VO<sub>2</sub> phase from 200 reflex (b) after: oxygen implantation (1), 30 min annealing (2), 30+180 min annealing (3).

The depth distribution of vanadium oxide phases was investigated using the SIMS method. The VO<sub>x</sub> film implanted with the medium oxygen dose was used for analysis after thermal annealing for 30+180 min, because this film has the highest TCR value. The depth dependences of the V, VO, V<sub>2</sub>O<sub>3</sub>, VO<sub>2</sub> and V<sub>2</sub>O<sub>5</sub> cluster signals are shown in Fig. 5.

It is seen that, in the 100 nm region, there is a sharp increase in the signals of VO<sub>2</sub> and V<sub>2</sub>O<sub>5</sub> cluster ions, while the signals of V and VO cluster ions are reduced. A slight increase in the V<sub>2</sub>O<sub>3</sub> signal is also observed. It is obvious that oxygen implantation leads to formation of numerous VO<sub>2</sub> and V<sub>2</sub>O<sub>5</sub> nuclei in the surface layer. The content of metal vanadium and vanadium monoxide phases significantly reduces.

SEM images show (Fig. 6) that the film annealing leads to formation of the surface microcrystalline structure. At the medium dose (Fig. 6a) of oxygen implantation the film has better crystallinity and larger crystal sizes than those in the high dose implantation case (Fig. 6b). These data are in good agreement with the X-ray data and confirm the thesis that the supersaturating

by oxygen slows down the crystallization of films. Thus, we have demonstrated that the low-temperature method to form vanadium oxide crystalline films [11, 12] can be used for ion-implanted films.

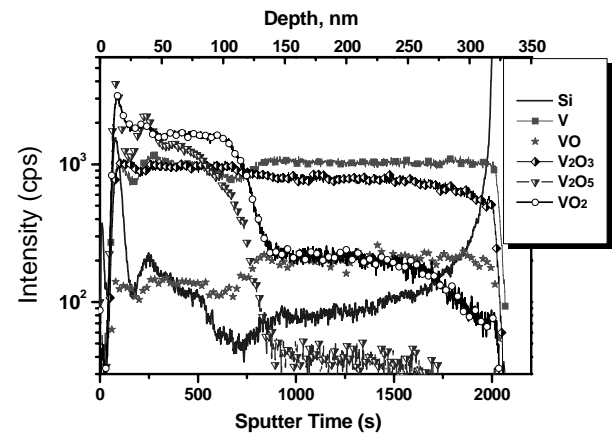


**Fig. 5.** TOF-SIMS depth profiles of Si, V, VO, V<sub>2</sub>O<sub>3</sub>, VO<sub>2</sub>, V<sub>2</sub>O<sub>5</sub> after implantation and annealing of the SiO<sub>x</sub> film.

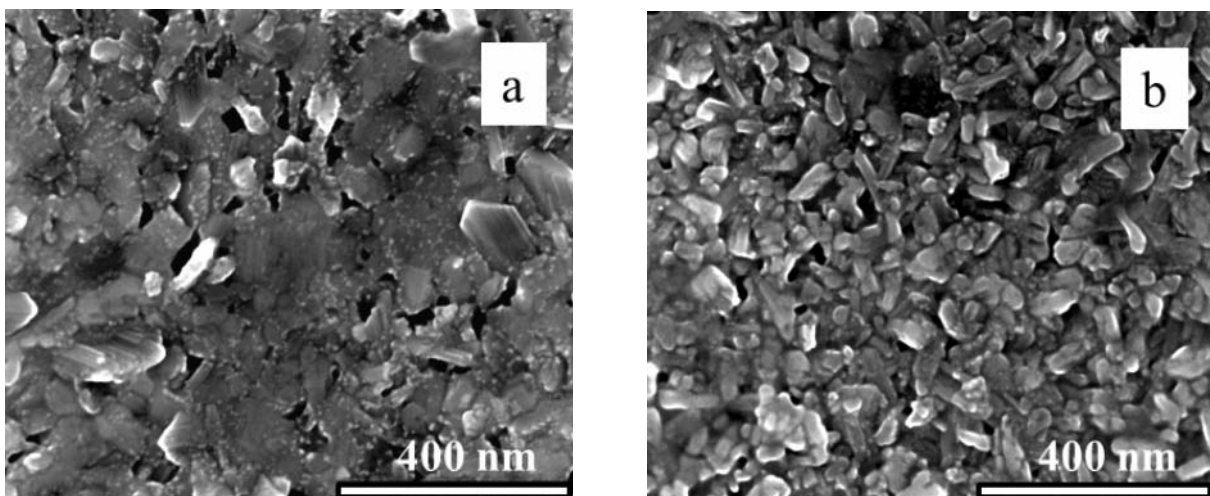


**Fig. 6.** SEM surface images of the film implanted with the medium (a) and high (b) doses after 30+180 min annealing.

As it was shown in [13], only amorphous films with rare nanocrystalline inclusions are the most suitable object for controlled crystallization and modification of crystals under the subsequent low-temperature annealing. Since the doses that we applied lead to complete amorphization of surface layer, therein should not be crystallites that could be nuclei for crystallization during annealing. Most likely that crystallization nuclei ( $V_2O_3$  crystallites) are located deeper ( $>100$  nm from the surface level) than the layer of ion penetration.

#### 4. Conclusion

It has been shown that the low-temperature (200 °C) of vanadium oxide films deposition results in the  $VO_x$  amorphous film formation with a high content of  $V_2O_3$  phase. Additional oxygen implantation creates an oxygen supersaturated region in the  $VO_x$  film with a smaller size of  $V_2O_3$  crystallites. Obviously, the subsequent low-temperature annealing leads to the shift of the film thermodynamic equilibrium state in direction to the formation of  $VO_2$  and  $V_2O_3$  crystallization centers. Prolonged low-temperature annealing leads to the growth of semiconductor crystals. Exactly these semiconductor phases can be responsible for this behavior of TCR described above. An excess of oxygen content above the critical level leads to the higher amorphization level and dissolution of the crystallization centers. In this case, an amorphous state of film with a smaller size of  $V_2O_3$  crystallites is more thermally stable. Thus, the used method enables to calculate and to inject the missed amount of oxygen in a film by ion implantation for obtaining the high TCR value.

#### References

1. Fieldhouse N., Pursel S.M., Carey R., Horn M.W., and Bharadwaja S.S.N. Vanadium oxide thin films for bolometric applications deposited by reactive pulsed dc sputtering. *J. Vac. Sci. Technol. A*. 2009. **27**, No. 4. P. 951–955.
2. Morin F.J. et al. Oxides which show a metal-to-insulator transition at the Neel temperature. *Phys. Rev. Lett.* 1959. **3**. P. 34.
3. Chen S.H., Ma H., Dai J., and Yi X.J. Nanostructured vanadium dioxide thin films with low phase transition temperature. *Appl. Phys. Lett.* 2007. **90**, No. 10. P. 101117.
4. Nadkarni G.S., Shirodkar V.S. Experiment and theory for switching in  $Al/V_2O_5/Al$  devices. *Thin Solid Films*. 1983. **105**. P. 115–129.
5. Zerov V.Yu., Kulikov Yu.V., Malyarov V.G. et al. Vanadium oxide films with improved characteristics for IR microbolometric matrices. *Techn. Phys. Lett.* 2001. **27**, No. 5. P. 378–380.
6. Booth J.M., Drumm D.W., Casey P.S. et al., Correlating the energetics and atomic motions of the metal-insulator transition of  $M1$  vanadium dioxide. *Sci. Repts.* 2016. **6**. P. 26391.
7. Viswanath B., Ko C., Ramanathan S. Size effects on stress relaxation across the metal insulator transition in  $VO_2$  thin films. *J. Mater. Res.* 2011. **26**. P. 1384.
8. Venkatasubramanian C., Cabarcos O.M., Allara D.L., Horn M.W., and Ashok S. Correlation of temperature response and structure of annealed  $VO_x$  thin films for IR detector applications. *J. Vac. Sci. Technol. A*. 2009. **27**, No. 4. P. 956–961.
9. Han Y.H., Kim K.T., Ahn N.C., Shin H.J. et al. Fabrication and characterization of bolometric oxide thin films based on vanadium tungsten alloy. *Sens. Actuator A-Phys.* 2005. **123-124**. P. 660–664.
10. Venkatasubramanian C., Horn M.W., and Ashok S. Ion implantation studies on  $VO_x$  films prepared by pulsed dc reactive sputtering. *Nucl. Instrum. Meth. Phys. Res. B*. 2009. **267**, No. 8-9. P. 1476–1479.
11. Melnik V., Khatsevych I., Goltvyanskyj Yu., Nikirin V., Romanyuk B. Kuchuk A., Popov V., Kladko V., Kuchuk A. Thermo-chromic properties of vanadium dioxide films obtained by magnetron sputtering. *Ukr. J. Phys.* 2011. **5**. P. 534-540.
12. Melnik V., Khatsevych I., Kladko V., Kuchuk A., Nikirin V., Romanyuk B. Low-temperature method for thermo-chromic high ordered  $VO_2$  phase formation. *Mater. Lett.* 2012. **68**. P. 215–217.
13. Goltvyanskyi Yu., Khatsevych I., Kuchuk A., Kladko V., Melnik V., Lytvyn P., Nikirin V., Romanyuk B. Structural transformation and functional properties of vanadium oxide films after low-temperature annealing. *Thin Solid Films*. 2014. **264**. P. 179–185.